A new pseudodeterministic multivariate receptor model for individual source apportionment using highly time-resolved ambient concentration measurements

Seung Shik Park,[1] J. Patrick Pancras, and John Ondov
Department of Chemistry and Biochemistry, University of Maryland, College Park, Maryland, USA

Noreen Poor
Department of Environmental and Occupational Health, College of Public Health, University of South Florida, Tampa, Florida, USA

[1]   A new multivariate pseudodeterministic receptor model (PDRM), combining mass balance and Gaussian plume dispersion equations, was developed to exploit highly time-resolved ambient measurements of SO_2 and particulate pollutants influencing air quality at a site in Sydney, Florida, during the Tampa Bay Regional Aerosol Chemistry Experiment (BRACE) in May 2002. The PDRM explicitly exploits knowledge of the number and locations of major stationary sources, source and transport wind directions, stack gas emission parameters, and meteorological plume dispersion parameters during sample collections to constrain solutions for individual sources. Model outputs include average emission rates and time-resolved ambient concentrations for each of the measured species and time-resolved meteorological dispersion factors for each of the sources. The model was applied to ambient Federal Reference Method SO_2 and 30-min elemental measurements during an 8.5-hour period when winds swept a 70° sector containing six large stationary sources. Agreement between predicted and observed ambient SO_2 concentrations was extraordinarily good: The correlation coefficient (R^2) was 0.97, their ratio was 1.00 ± 0.18, and predicted SO_2 emission rates for each of four large utility sources lie within 8% of their average continuous emission monitor values. Mean fractional bias, normalized mean square error, and the fractions of the predictions within a factor of 2 of the observed values are -2.7, 0.9, and 94%, respectively. For elemental markers of coal-fired (As and Se) and oil-fired (Ni) power plant emissions the average ratio of predicted and observed concentrations was 1.02 ± 0.18 for As, 0.96 ± 0.17 for Se, and 0.99 ± 0.41 for Ni, indicating that the six sources located in the wind sector between approximately 200° and 260° well accounted for background-corrected concentrations measured at the sampling site. Model results were relatively insensitive to the choice of upper bound used to constrain solutions.

1. Introduction

[2]   Source apportionment, i.e., quantitative determination of the contributions of pollutants from their sources to ambient atmospheric levels, is necessary for developing emission control strategies that effectively reduce exposures and health risks, and prevent degradation of air quality [*Gordon*, 1988]. Source attribution may be accomplished with either source- or receptor-based models, however, applications of the former are often limited because of the lack of emission rate data. In the latter, source contributions are determined using observations at sampling (i.e., receptor) sites. Receptor models are typically of three types, i.e., those that make use of no information other than ambient meteorological and concentration measurements (e.g., factor analysis (FA) methods such as principle component analysis (PCA)); those that require a single unique tracer for each source (multilinear regression. MLR); and those requiring detailed information on the relative abundances of pollutants emitted from each source (i.e., source "profiles," e.g., chemical mass balance (CMB)). Of these, CMB has been the most robust, as it traditionally makes use of more information about the sources than do the other methods.

---

[1]Now at Department of Environmental Engineering, Chonnam National University, Gwangju, Korea.

Additionally, traditional FA methods suffer from "rotational ambiguities" resulting from transformation of abstract eigenvectors into concrete source compositions [*Henry*, 1987], and they cannot resolve sources whose ambient concentrations become correlated by virtue of spatial/meteorological colinearity. More recently, advanced FA models seek to remove rotational ambiguity by estimating solutions to the inherent mass balance equations by least squares minimization, e.g., positive matrix factorization (PMF) [*Paatero*, 1997] and Constrained Physical Receptor Model (COPREM) [*Wahlin*, 2003]. The most advanced models limit the universe of possible solutions by employing nonnegativity criteria [*Paatero*, 1997] and/or constraints on stoichiometry and range of source composition variables (UNMIX) [*Henry*, 2000; *Kim and Henry*, 2000; *Henry and Norris*, 2002]. Unlike PMF, UNMIX estimates the number of factors and the composition and contributions of these factors to the particulate loadings [*Henry et al.*, 1999; *Kim and Henry*, 2000]. Also, both source compositions and contributions are constrained to positive values. Moreover, both COPREM and Multilinear Engine (ME) [*Paatero*, 1999] allow flexible input of "profiles" for one or more sources when known, while allowing solutions for the remaining unknown "profiles." Despite these advances, none of these models truly makes use of much commonly available, but important information, e.g., numbers and locations of known sources and their relationships with wind angle.

[3] Until recently, most of the data obtained for receptor modeling has been derived from samples collected over timescales far longer than those for changes in source strengths and important meteorological parameters, e.g., wind direction and mixing height. The accompanying homogenization of source signals by this practice severely reduces the resolving power achievable with FA methods [*Lioy et al.*, 1989]. At 2-hour resolution, *Rheingrover and Gordon* [1988] demonstrated that plumes of stationary sources in St. Louis are readily observed as excursions in time series profiles of the concentrations of the various marker elements. More recently, *Kidwell and Ondov* [2001, 2004] have described a system for measuring elemental constituents at 30-min intervals, allowing for improved source resolution under more variable wind conditions [*Ondov et al.*, 2003]. Such data contain substantial information on the locations of specific sources. Aside from correlating peaks with wind direction, more distant sources produce temporal excursions of longer duration than do nearby sources. These differences are revealed when winds shift direction. Despite advances, information such as this, which is provided by highly time-resolved data, has not been fully exploited in receptor modeling.

[4] Gaussian plume-based dispersion models [*Pasquill*, 1961; *Gifford*, 1961; *Schwede and Paumier*, 1987; *Hanna et al.*, 2003] have been applied widely for estimating mean pollutant concentrations resulting from point source releases because of their simplicity [*U.S. Environmental Protection Agency* (*U.S. EPA*), 1980]. These models incorporate off-axis decay of concentrations from their maxima along the plume centerline and are commonly used to evaluate potential effects of primary emissions from industrial stacks. Much earlier, both *Cooper* [1982] and *Yamartino* [1982] described hybrid receptor models in which measured concentrations were reconciled against the products of emission rates and dispersion factors determined from a Gaussian plume dispersion model. These attempts met with limited success, owing in part from the lack of highly time-resolved data for many species, but largely because of errors in the Gaussian plume model.

[5] Herein, we describe a new pseudodeterministic multivariate hybrid receptor model (PDRM), wherein the Gaussian plume model is used to constrain solutions to the mass balance receptor equation. The purpose is to exploit directionality and plume dispersion information inherent in highly time-resolved ambient concentration data now available to resolve the contributions of primary pollutants emitted from stationary sources. Unlike traditional receptor models, the PDRM exploits knowledge of the number and locations of major stationary sources, source and transport wind directions and distances, stack gas emission parameters, and meteorological plume dispersion during sample collections. Furthermore, emission rates are predicted for specific, individual sources.

[6] The model and its application to elemental composition measurements made at 30-min intervals with the University of Maryland Semicontinuous Elements in Aerosol Sampler (SEAS) in Sydney, Florida, during the Bay Regional Aerosol Chemistry Experiment (BRACE) are described below.

2. Experimental Data
2.1. Study Area and Modeling Period

[7] As shown in Figure 1, the Sydney site is located at the intersection of Dover and Sydney roads near Valrico, Florida. The site is surrounded by major freeways such as I-4 (due north, 6 km), I-75 (due south, 9.5 km), and Highway 60 (due south, 2 km), and several anthropogenic industrial sources. Our modeling was performed on ambient data collected between 1200 and 2100 local time (LT) on 13 May 2002, during which time wind angles (measured from true north) ranged from $200°-270°$ and hourly averaged wind speeds ranged from 1 to 4 m/s (see Figure 2). This sector contains four large electric utility coal- and oil-fired power plants, specifically, the Manatee plant operated by Florida Power and Light (FPL), Tampa Electric Company's (TECO) Big Bend and FJ Gannon plants, and Progress Energy's (PE, formally Florida Power's) PT Bartow plant; and two industrial sources (Cargill Fertilizer and Gulf Coast Recycling). Fuel type, source-receptor distances and station angles (measured at Sydney from due north), and emissions data for PM and SO_2 are listed in Table 1. As indicated, the Manatee oil-fired power plant is located at an angle (station angle) of $196°$, 41 km away from the site. The Big Bend and Gannon coal-fired power plants were located at respective station angles and distances of $220°$ and $251°$ and 25 and 20 km (note that the FJ Gannon plant no longer exists: it has been replaced with a natural gas-fired combined cycle power plant and renamed as Bayside). Their generating load capacities were ~1800 and 1200 MW, respectively. The stacks at the Big Bend plant, however, are equipped with both an electrostatic precipitator (ESP) and a wet (forced oxidation lime) scrubbers; hence SO_2 emissions from Gannon are larger despite its smaller size. The Gannon power plant is equipped with ESPs and SO_2 emissions are controlled through the use of low-sulfur coal.
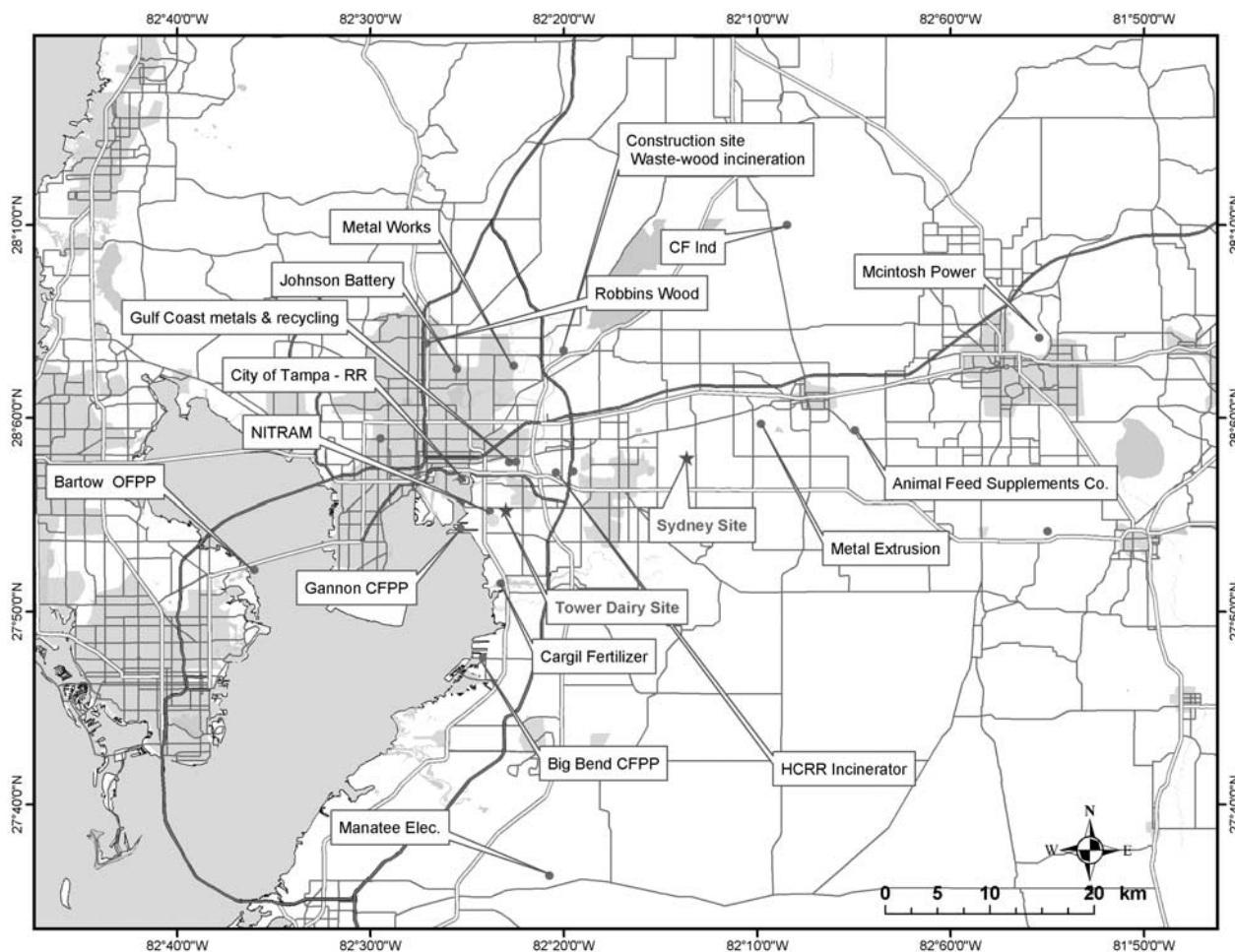
Figure 1. Area map showing the Sydney sampling site and nearby air emission sources. See color version of this figure at back of this issue.

Bartow is an oil-fired power plant and is located 38 km upwind at 253°. Its SO_2 emissions are about two thirds those of Manatee and less than one half those from Gannon. Particle emissions from one of three stacks of Bartow is controlled by an ESP. The Cargill fertilizer plant burns sulfur to make sulfuric acid and also burns natural gas in its other heating operations. It emits ~3500 t of SO_2 annually. The Gulf Coast lead-battery-recycling plant burns coke in its blast furnace and natural gas in its other melting operations. The recycling plant emits ~500 t of SO_2 annually.

[8] Hourly SO_2 emission rates for the four utility power plants were obtained from the EPA's Clean Air Markets Emissions Data and Compliance Report web page (available at http://www.epa.gov/airmarkets/emissions/index.html) and are plotted in Figure 3. Annual SO_2 emission rate estimates for the Cargill and Gulf Coast plants were provided by the Florida Department of Environmental Protection. As indicated in Figure 3, SO_2 emission rates from each of the stacks were fairly constant over the study period except for Manatee. For example, SO_2 emission rates for Gannon were in the range 9100–9800 kg/h with a mean of 9400 kg/h. This is the optimum condition for estimating the emission rates of SO_2 from the plant because, as described below, the emission rate term in the governing mass balance equation

(equation (1)) is assumed to be constant over the modeling period. However, for the Manatee plant the SO_2 release rate was substantially more variable, ranging from 3900 to 6200 kg/h with an average of 4600 kg/h.
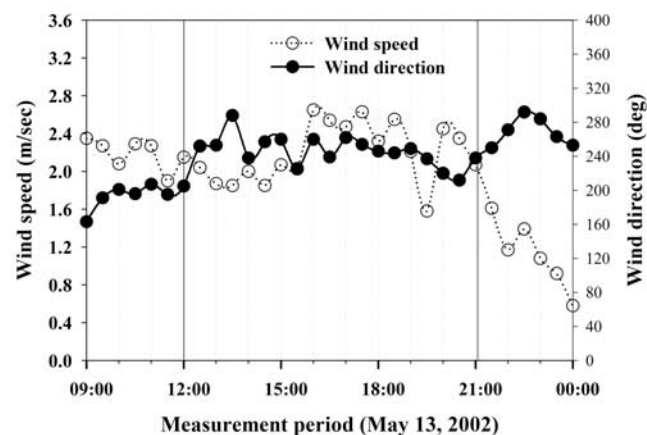

Figure 2. Profiles of wind speed and wind direction on 13 May 2002.

Table 1. Emission Source Information[a]

Plant Name	Fuels in Use	Control Technology	Distance, km	Station Angle, deg	PM, t/yr	SO$_2$ Emission
FPL Manatee	oil		41	196	9472	31,136[b]/1280[c]
TECO Big Bend	coal	ESP + wet scrubber	25	220	7591	12,095/303
Cargill Fertilizer	sulfur/NG		20	235	288	3422/40[d]
TECO Gannon	coal	ESP	20	251	6267	49,532/2610
FPC Bartow	oil		38	253	2600	23,200/1100
Gulf Coast Recycling	coke/NG		15	269	26	487/25[d]

[a]Distance, distance between the source and receptor sites; station angle, angle between the receptor and source; PM, particulate matter; ESP, electrostatic precipitator; NG, natural gas.
[b]Metric tons (t/yr) of SO$_2$ emitted in 2001.
[c]Average value (g/s) of SO$_2$ continuous emission data between 1200 and 2100 LT, 13 May 2002.
[d]Annual average rate of SO$_2$ emission.

2.2. Meteorological Measurements

[9] Two-minute averaged surface meteorological observations were available from a National Oceanic and Atmospheric Administration (NOAA) vertical profiling site at Sydney (NOAA Environmental Technology Laboratory, inactive site archives, edited data, available at http://www.etl.noaa.gov/et7/data/). Thirty-minute averages of the NOAA wind speed and direction measurements made during the study period on 13 May are shown in Figure 2. In the predawn hours, the temperature and relative humidity averaged 20°C and 98%, respectively, with light winds from the southeast under stable atmospheric conditions. As the sun rose on the horizon, the winds shifted clockwise and developed into a southwesterly flow off of Tampa Bay. The midday high temperature and low relative humidity averaged 33°C and 37%, respectively, with strong convective mixing. The mixing height reached an estimated 2400 m by midafternoon under neutral atmospheric conditions and with more westerly winds at 3–4 m/s off of Tampa Bay. Westerly winds continued through the evening, with lower wind speeds and stable atmospheric conditions developing within an hour after sunset. Sunrise was at 0541 eastern standard time (EST), and sunset was at 0711 EST. No precipitation was recorded across the Tampa Bay area.

[10] In addition to surface wind observations available at the Sydney site, SSESCO, Inc. (St. Paul, Minnesota) produced CALMET 5.22 model (Level 020828) input files for a 600 × 900 km modeling domain over peninsular Florida on a 10-km grid scale with 12 vertical layers, as part of the Bay Regional Atmospheric Chemistry Experiment (BRACE) effort. They began with the three-dimensional meteorological fields from an archived NOAA North American Rapid Update Cycle (RUC2) prognostic model, which assimilates surface and upper air observations, satellite and radar data into a weather forecast. The RUC2 model was run with a 1-hour resolution for 40 km grid cells and 40 vertical layers and was used as a first guess for a mesoscale data assimilation using the Advanced Regional Prediction System (ARPS) Data Assimilation System (ADAS) and METAR observations. The resulting mesoscale temperature, pressure, wind and humidity fields were checked by SSESCO with an objective data analysis technique and used in CALMET as a first-guess wind field and as virtual surface and upper air observations spaced across the modeling domain for the CALMET objective analysis procedure. The CALMET model includes a diagnostic wind field generator and a micrometeorological model for overland and overwater boundary layers and produces, as output, hourly winds and temperatures for a three-dimensional modeling domain and hourly two-dimensional outputs of mixing heights and surface characteristics [Scire et al., 2000]. The Pasquill stability class, mixing height, friction velocity, Monin-Obukhov length, and convective velocity scale were obtained from the CALMET output at the geo-coordinates of the Sydney site and used in the PDRM as described below.

2.3. SO$_2$ and Elemental Measurements
2.3.1. SO$_2$

[11] Ambient SO$_2$ mixing ratios (ppb) were measured with a federal reference method "pulsed fluorescence analyzer" (PFA) at 1-min intervals during the study period. These were converted to μg/m^3 using ambient temperature and pressure data and used to construct 30-min averages for use in the PDRM. Examination of the SO$_2$ data reveals that at least three transients occurred during the study period. The highest 30-min averaged SO$_2$ concentration, 41.1 ppb (106 μg/m^3), was observed at 1830 LT on 13 May.

2.3.2. PM$_{2.5}$ Metal Sampling and Elemental Analyses

[12] As described by Pancras [2005], ambient aerosol collections were made at Sydney during the study period, using the University of Maryland Semi-continuous Elements in Aerosol Sampler (SEAS). The SEAS consists of a state-of-the-art dynamic aerosol concentrator mated to an automated sample collector. Detailed descriptions of the SEAS sampler have been presented elsewhere [Kidwell and Ondov, 2001, 2004; Pancras, 2005]. Successive 30-min samples were collected routinely from 1 to 31 May 2002,
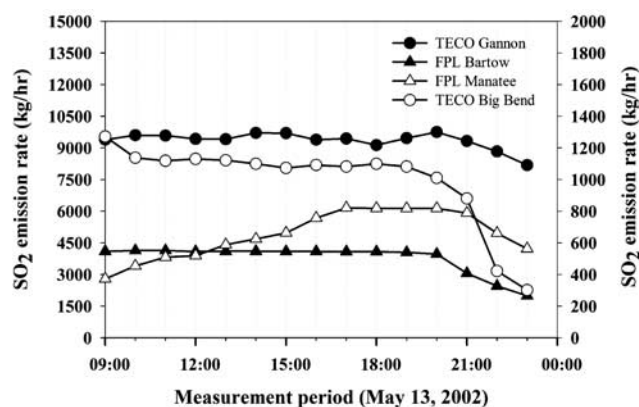

Figure 3. Actual SO$_2$ emission rates for four power plants in the study area.

Table 2. Stack Information Used in the Model

Plant Name	Stack Height, m	Stack Internal Diameter, m	Stack Exit Temperature, K	Stack Exit Velocity, m/s
FPL Manatee	152	7.9	436	25
TECO Big Bend	152	7.3	410	15
Cargill Fertilizer	46	2.5	345	11
TECO Gannon	96	4.5	423	23
FPC Bartow	91	3.3	408	34
Gulf Coast Recycling	46	0.9	344	17

resulting in a total of >700 samples. A subset of these, including 18 of those collected during the 13 May study period, were analyzed in triplicate by simultaneous multi-element graphite furnace atomic absorption spectroscopy (GFAAS) with Zeeman background correction (SIMMA 6000, Perkin Elmer Corp., Danbury, Connecticut) for Al, As, Cd, Cr, Cu, Fe, Mn, Ni, Pb, Se, and Zn. Additional details, including quality control/quality assurance protocols, are given by *Pancras* [2005].

[13] The PDRM is designed specifically to apportion contributions from stationary sources whose plumes induce excursions in concentrations above the background levels induced by observed at a single receptor location. Therefore background concentrations were evaluated and subtracted prior to use in the PDRM. These were as follows: SO_2, 0.52 $\mu g/m^3$; Al, 25.0 ng/m^3; As, 0.10 ng/m^3; Cr, 0.13 ng/m^3; Cu, 0.45 ng/m^3; Fe, 6.76 ng/m^3; Mn, 0.48 ng/m^3; Ni, 0.53 ng/m^3; Pb, 0.37 ng/m^3; Se, 0.10 ng/m^3; and Zn, 1.72 ng/m^3. (Background corrected concentrations for SO_2 and each of the 10 elemental particle constituents are shown in Figures 7 and 8.) When run with non-background-subtracted data, model results were nearly identical to those obtained using the background-subtracted data.

3. Model Description

3.1. Least Squares Model

[14] Our goal is to determine the emission rates of species, i, from j stationary sources, using highly time-resolved concentration measurements from the SEAS and SO_2 monitors. The basis of the model is a mass balance equation such that the ambient contributions of each of the sources to each species are expressed as products of emission rates ($ER_{i,j}$, g/s) and meteorological dispersion factors ($\chi/Q_{j,t}$, s/m^3) appropriate for each for each sampling period, t, i.e.,

$$[E_i]_t = \sum_{j=1}^{n} ER_{i,j}(\chi/Q)_{j,t} \qquad (1)$$

where $[E_i]_t$ denotes the measured concentration of the species of interest at the receptor site and $ER_{i,j}$ represent averages for the period during which the samples (time intervals) used in model were collected. To solve the model, $(\chi/Q)_{j,t}$ are calculated for each sampling interval using a simple Gaussian plume model,

$$(X/Q)_{j,t}^{Met} = \frac{1}{\pi \sigma_y \sigma_z u} \exp^{-\frac{1}{2}\frac{y^2}{\sigma_y^2}} \cdot \exp^{-\frac{1}{2}\frac{H^2}{\sigma_z^2}} \qquad (2)$$

In equation (2), χ is the concentration (g/m^3) of gas or aerosols at ground level (i.e., $z = 0$) from a continuous

source with an effective emission height, H; Q is the continuous mass emission rate (g/s); and u is the transport wind speed (m/s) representing the speed of the plume over its trajectory. Dispersion parameters, σ_y and σ_z, are the standard deviations of the concentration distributions in the lateral (y) and vertical (z) directions, and increase with downwind distance from the source (x). It is assumed that all emitted species are conserved, i.e., are neither removed by gravitational settling, dry or wet deposition, nor by chemical reactions.

[15] Equations (1) and (2) are those used by *Yamartino* [1982], but in our implementation, equation (1) is solved using a nonlinear least squares solver ("lsqcurvefit") in MATLAB (MathWoks, Inc, version 6.5) in which equation (2) is employed to constrain equation (1). The MATLAB program provides a solution that minimizes an object function, FUN, which we define as follows:

$$FUN = \sum_{i=1}^{l} \sum_{t=1}^{m} \sum_{j=1}^{n} \left(ER_{i,j}(\chi/Q)_{j,t} - [E_{i,t}] \right)^2 \qquad (3)$$

which is solved with the constraint that

$$LB(\chi/Q)_{j,t}^{Met} \le (\chi/Q)_{j,t} \le UB(\chi/Q)_{j,t}^{Met},$$

where LB and UB are upper and lower bounds reflecting uncertainty in the Gaussian plume model.

[16] Input variables used in the hybrid receptor model are as follows: (1) 30-min ambient concentrations of SO_2, Al, As, Cr, Cu, Fe, Mn, Ni, Pb, Se, and Zn, (2) derived and measured meteorological parameters, as described below, (3) stack data (physical stack height, stack inside diameter, exit gas velocity, and exit gas temperature (see Table 2), and (4) station angles for the six emission sources.

[17] Setting up constraints is essential to the hybrid receptor model because the number of solutions for a product of unknowns is infinite. Once configured, the constrained model was applied to estimate the emission rates of SO_2 and elemental constituents of primary particles. The results for SO_2 are evaluated by comparison against continuous emission monitoring data available for four of the sources and annual emission estimates for the two smaller sources, i.e., Cargill and Gulf Coast.

[18] Initially, solutions for $(\chi/Q)_{j,t}$ were constrained to the range 0.1–2.0, consistently, for all six sources. This choice was derived from information reported for an intentional tracer study [*Ondov et al.*, 1992] conducted at a coal-fired power plant 20 km from an arc of samplers in Maryland, a location for which terrain and land use are somewhat similar to that of Tampa, in which χ/Q calculated with two different parameterizations of a Gaussian plume model differed by a factor of 5–10. However, as discussed below, the model

was also run using separate constraints for the Cargill and Gulf coast plants, and sensitivity analyses were performed. As described below, the former choice produced ERs that exceeded their reported annual emission rates by factors of >3 and >12 for Cargill and Gulf coast, respectively. These results might well be accurate, but effective plume heights (<100 m) for these plants are low (compared with, for example, those for the Manatee Plant, for which the effective plume height was 1200 m during the period of influence at the receptor site) and dispersion of their plumes is expected to be more affected by surface roughness elements than those from the larger plants. For these reasons, we applied separate LB and UB constraints for these two sources and reran the model. Initial choices for LB and UB for Cargill were 0.4 to 8 and 1.2 to 24 for Gulf coast. Results for both models runs, as well as the sensitivity analysis, are discussed below.

3.2. Gaussian Dispersion Parameters (σ_y and σ_z)

[19] The values of σ_y and σ_z vary with turbulence, height above the surface, surface roughness, and downwind distance from the source and, hence, transport wind speed and time. Herein, σ_y and σ_z were determined from correlations developed by *Draxler* [1976] and *Irwin* [1979] as follows:

$$\sigma_y = \sigma_v t F_y \qquad (4)$$

$$\sigma_z = \sigma_w t F_z \qquad (5)$$

where σ_v and σ_w are the standard deviations of the wind velocity in the y and z directions, respectively, t is the travel time from the source to the location of interest, and F_y and F_z are universal functions of parameters that specify the characteristics of the atmospheric boundary layer. Specifically, these are friction velocity, u^*; the Monin-Obukhov length, L; the mixed layer depth, z_i; the convective velocity scale, w_*; the surface roughness, z_o; and the effective stack height, z, i.e., the height of pollutant release above the ground. Different formulae are used for different stability classes [*Draxler*, 1976; *Binkowski*, 1979; *Irwin*, 1979]. Likewise, σ_v and σ_w are calculated from friction velocity (u^*) and L, using formulae appropriate for different stability classes. Hourly values of the Pasquill stability class, z_i (m), u^* (m/s), L (m) and w_* (m/s), were obtained from the CALMET model [*Scire et al.*, 2000] output at the geocoordinates of Sydney, Florida, as described above. These were interpolated to produce half-hourly estimates for use in the model. A surface roughness length of 0.25 m was used in this analysis.

3.3. Transport Wind Velocity u

[20] The wind profile power law was used to estimate horizontal transport speed, u, at the effective plume height, z, given the horizontal surface wind speed, u_1, at height z_1 (i.e., the 10 m, meteorological tower height). The power law equation is of the form

$$u = u_1 (z/z_1)^p \qquad (6)$$

where p is given by equation (6) [*Panofsky et al.*, 1960].

$$p = \frac{\phi_m\left(\frac{z}{L}\right)}{\frac{U\kappa}{u_*}} \qquad (7)$$

where the nondimensional wind shear, $\phi_m(z/L)$, and the nondimensional wind speed, $U\kappa/u_*$, are universal functions; and k is the von Karman constant, which is equal to 0.4. Equation (5) is invalid for wind transport speeds less than 1.0 m/s. Therefore a minimum value of 1.0 m/s was used.

[21] Transport speeds calculated in this manner were relatively constant during the 9-hour modeling period. Thus the transport speed was calculated for each 30-min interval and an average transport speed was used in the receptor model. Likewise, transport time was calculated from the average transport speed at stack height and source-to-receptor site distance. Transport times were assumed to be constant over the 9-hour period, despite shifts in the wind angle, which lead to differences in x for each source.

3.4. Effective Plume Height H

[22] The plume height is used in the calculation of the vertical term described in equation (2) and in calculating the transport velocity, as described above. The effective stack height is taken to be the sum of the actual stack height (h_s) and the plume rise (ΔH).

$$H = h_s + \Delta H \qquad (8)$$

Herein, plume rise (ΔH) is calculated by the formulas expressed by *Briggs* [1969, 1971, 1974] and *U.S. EPA* [1995]. The detailed mathematical formulas can be found in Briggs' papers, and a brief description is given below. The effective stack height (H) is determined for conditions at the stack exit. If the plume is dominated by buoyancy, the buoyancy flux parameter, F_b (m^4/s^3), is given by

$$F_b = g v_s d_s^2 \left(\frac{\Delta T}{4T_s}\right) \qquad (9)$$

where g is gravitational acceleration (m/s^2), v_s is the stack gas exit velocity (m/s), d_s is the inside stack top diameter (m), u_s is mean wind speed (m/s) at stack height, $\Delta T = T_s - T_a$, T_s is the stack gas temperature (K), and T_a is the ambient air temperature (K).

[23] The plume height (H) for unstable or neutral atmospheric conditions is determined by two different flux parameters: (1) For $F_b < 55$,

$$H = h_s + 21.425 \frac{F_b^{3/4}}{u_s} \qquad (10)$$

(2) For $F_b \geq 55$,

$$H = h_s + 38.71 \frac{F_b^{3/5}}{u_s} \qquad (11)$$

The plume height (H) for stable atmospheric conditions is given by equation (11)

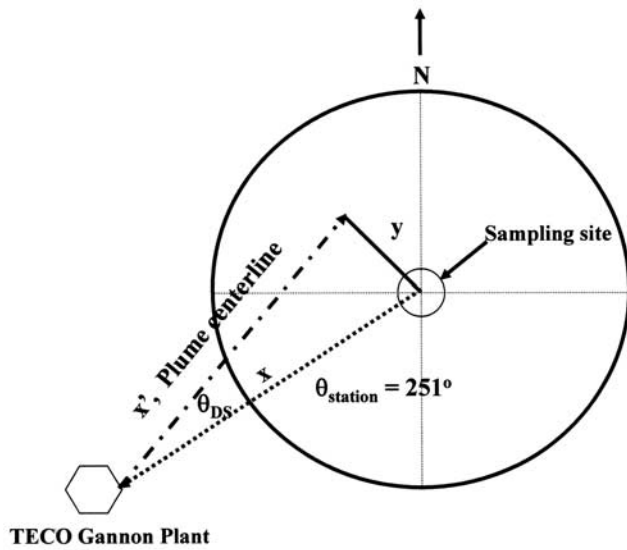$$H = h_s + 2.60 \left(\frac{F_b}{u_s s}\right)^{1/3} \qquad (12)$$

Figure 4. The PDRM makes use of source angle and distance relationships. Plume transport distance (x') and displacement (y) of the plume centerline from the sampling site are shown.

If the plume is dominated by momentum, the momentum flux parameter, F_m (m^4/s^3), is given by

$$F_m = v_s^2 d_s^2 \left(\frac{T_a}{4T_s}\right) \tag{13}$$

The plume height (H) for an unstable or neutral atmospheric condition is given by

$$H = h_s + 3.0 \quad d_s \frac{v_s}{u_s} \tag{14}$$

The plume height (H) for a stable atmospheric condition is given by

$$H = h_s + 1.5\left(\frac{F_m}{u_s\sqrt{s}}\right) \tag{15}$$

where s (= $g(\partial\theta/\partial z)/T_a$) is a stability parameter indicating the potential temperature gradient with height.

[24] Emission parameters required to calculate the effective plume height (H) in the Gaussian plume dispersion equation (2) are listed in Table 2.

3.5. Distance Between the Plume Centerline and the Sampling Site (y)

[25] According to equation (2), the plume concentration decays exponentially with increasing distance, y, from the plume centerline. As illustrated in Figure 4, wherein x' is the plume transport distance, y is related to the deviation, θ_{DS}, between the wind angle, θ_{wind}, and station angle, $\theta_{station}$, and the source-to-sampling site distance, x, as follows:

$$y = \sin\ \theta_{DS} \cdot x \tag{16}$$

$$\theta_{DS} = \theta_{station} - 180° - \theta_{wind} - \theta_{Ekman}$$

where θ_{Ekman} is the wind angle rotation at transport height relative to the surface wind direction (in degrees) due to the Ekman effect. In Figure 4, we show a station angle (251°) corresponding to the TECO Gannon power plant. Both θ_{wind} and $\theta_{station}$ are measured from true north. In the model, we used an average wind angle, computed from the 15-min surface wind data measured at the meteorological tower, i.e., averaged during the period of transport for each source (case 2).

4. Results and Discussion

4.1. Volumetric Dispersion Factors (χ/Q) and SO$_2$ Emission Rates

[26] As applied to the data of 13 May, the model was solved to obtain a set of 66 emission rates (i.e., 11 species for each of the six sources) and for a set of 108 dispersion

Table 3. Predicted Emission Rates of SO$_2$ and Metal Species[a]

Species	Gannon	Bartow	Big Bend	Manatee	Cargill	Gulf Coast
SO$_2$ (observed)[b]	2600 ± 50	1140 ± 10	300 ± 10	1360 ± 300,1110[c]	40[d]	25[d]
SO$_2$ (predicted)	2590[e] (2510)[f]	1030 (1130)	320 (290)	1140 (1045)	130 (49)	340 (31)
Al	1.109 (1.000)	0.151 (0.522)	1.229 (1.131)	6.946 (7.577)	0.058 (0.204)	0.042 (0.582)
As	0.031 (0.030)	0.032 (0.032)	0.019 (0.018)	0.006 (0.001)	0.001 (0.001)	0.001 (0.004)
Cr	0.029 (0.024)	0.027 (0.022)	0.026 (0.027)	0.167 (0.226)	0.002 (0.007)	0.001 (0.011)
Cu	0.005 (0.018)	0.004 (0.015)	0.036 (0.031)	0.085 (0.117)	0.003 (0.007)	0.001 (0.014)
Fe	1.146 (1.084)	0.401 (0.534)	1.246 (1.147)	5.853 (6.725)	0.077 (0.270)	0.041 (0.520)
Mn	0.003 (0.011)	0.002 (0.010)	0.022 (0.020)	0.180 (0.214)	0.001 (0.002)	0.001 (0.011)
Ni	0.002 (0.010)	0.002 (0.011)	0.032 (0.060)	0.604 (0.650)	0.002 (0.002)	0.001 (0.007)
Pb	0.007 (0.033)	0.006 (0.028)	0.067 (0.057)	0.138 (0.166)	0.004 (0.008)	0.003 (0.035)
Se	0.032 (0.033)	0.032 (0.032)	0.002 (0.002)	0.043 (0.053)	0.001 (0.002)	0.001 (0.003)
Zn	0.018 (0.058)	0.018 (0.057)	0.113 (0.095)	0.760 (0.980)	0.005 (0.014)	0.003 (0.032)

[a]Units are in g/s.
[b]Average continuous emission monitor data from the stacks (1200~2100 LT, 13 May).
[c]Average emission rate during period of plume influence.
[d]Annual average SO$_2$ emission data in 1998 (not CEM data).
[e]Predicted SO$_2$ emission rates when all six sources identically constrained to the range 0.1–2.0 (case 1).
[f]Values in parentheses are predicted SO$_2$ emission when constraints for Cargill and Gulf Coast are set to 4 and 12 times those for the base constraint set for the other plants (case 2).
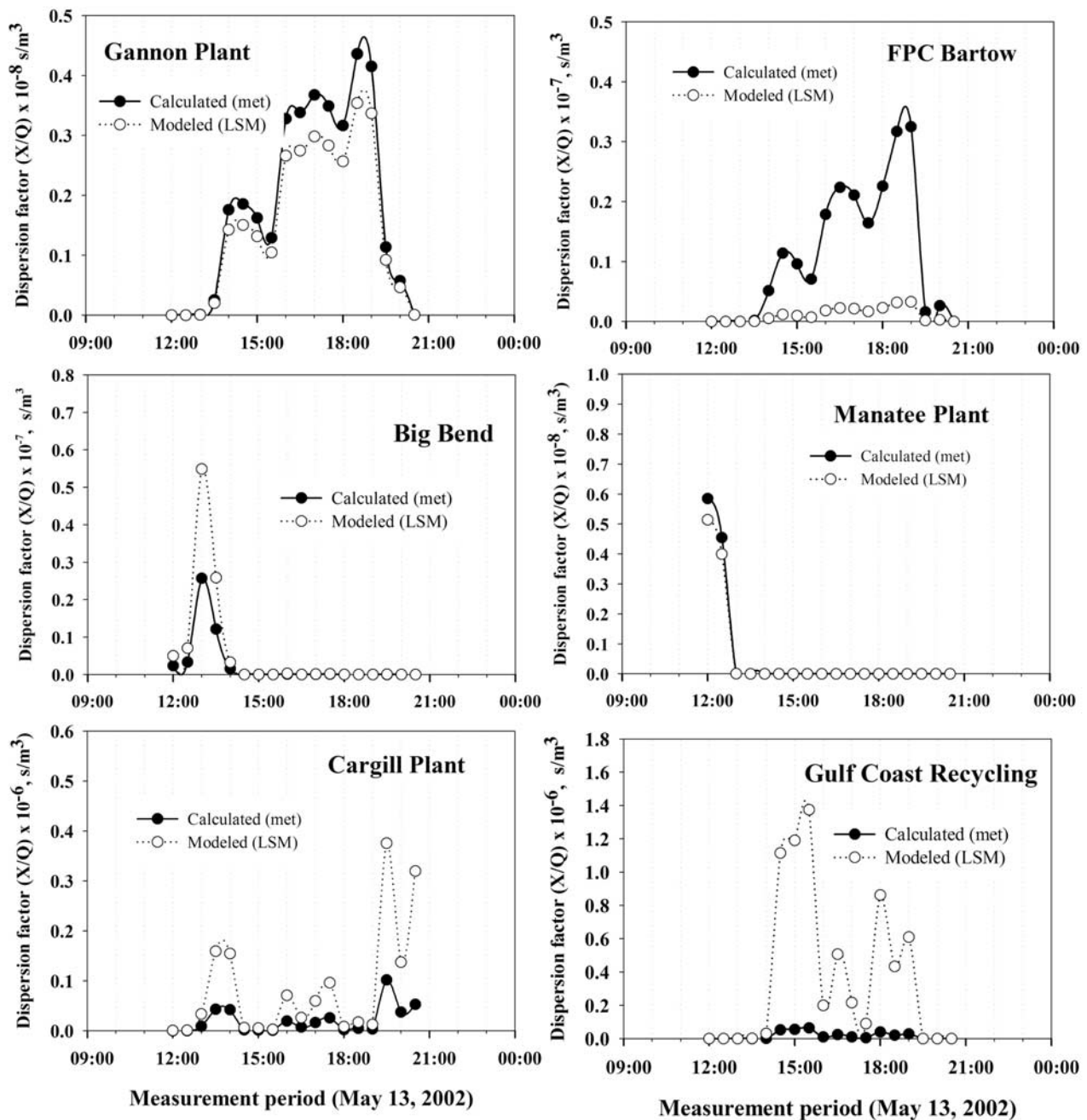
Figure 5. Comparison of dispersion factors (χ/Q) calculated with the meteorological model with those obtained from the least squares model for each of the sources for case 2, wherein constraints for Cargill and Gulf Coast are set to 4 and 12 times those for the base constraint set for the other plants.

factors (χ/Q^{PDRM}; 18 for each of the six sources). Results for both constraint strategies are listed in Table 3. The χ/Q predicted for case 2, i.e., where constraints for Cargill and Gulf Coast are set to 4 and 12 times those for the base constraint set for the other plants, are shown in Figure 5. In Figure 5, the χ/Q predicted by both the PDRM and Gaussian plume model (equation (2)) for each of the six sources are plotted as a function of time of day. As shown, χ/Q varied with each of the sources and time of day, as winds shifted the plume toward and away from the receptor site. The χ/Qs represent factors for which multiplication by

the emission rates give ambient concentrations. For the power plants, SO_2 emissions were relatively constant during their respective periods of influence on SO_2 levels at Sydney. Thus the values of χ/Q in Figure 5 are proportional to the induced ambient SO_2 concentrations and show when the plumes of the various stationary sources arrived. The Gannon plant, located 20 km from the site, had the largest SO_2 emissions (Table 1) and its plume strongly influenced the site between 1330 and 1930 LT. The plume was clearly influential on three occasions during the study period, i.e., at 1430, 1700,
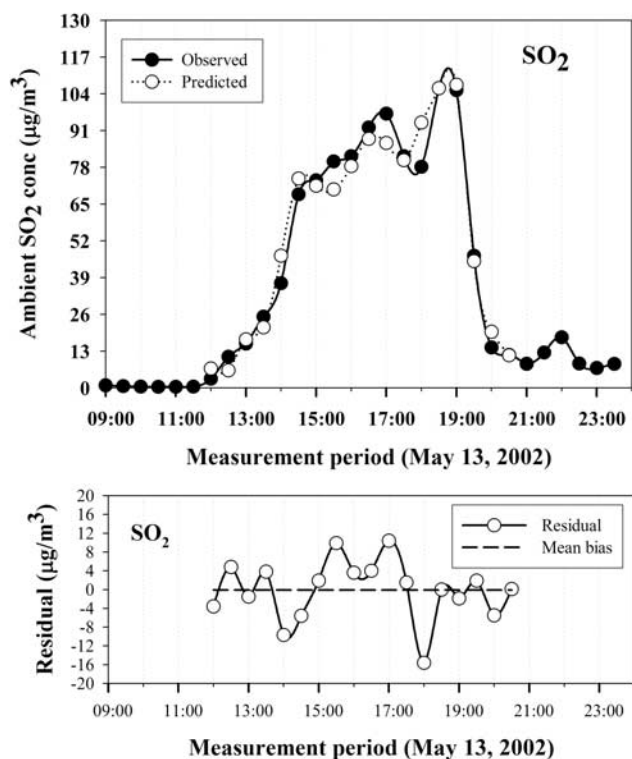
Figure 6. Comparison of observed and PDRM-predicted ambient SO$_2$ concentrations.

and 1830 LT. Maximum influence occurred at 1830 LT, which precisely corresponds to the time of the maximum SO$_2$ concentration (106 μg/m^3; see Figure 6). The profile for the χ/Qs for Bartow, located at nearly the same station angle, but 18 km more distant than Gannon, was very similar, but as indicated, the arrival of its plume (approximately 1400 LT) was delayed by approximately 30 min later than that of Gannon, in good agreement with its longer transport time (note that stack heights for the two plants were nearly identical).

[27] For Gannon, χ/Qs calculated with the meteorological model were quite similar to, but generally about 30% greater than, those predicted by the PDRM. For Bartow, χ/Qs predicted by the PDRM (χ/Q^{PDRM}) were roughly tenfold smaller than those for Gannon during the same periods, indicating more substantial plume dilution, owing to the greater distance of the former. Meteorological χ/Qs, however, for Bartow were at most twofold lower than those for Gannon, and differed less after 1800 LT. As described above, the relative small differences in dispersion over the additional 18 km transit probably reflects the neutral and later stable atmospheric conditions input into the Met model. However, the PDRM predictions are clearly more accurate, as can be seen from Table 3, wherein SO$_2$ emission rates for both Gannon (2600 g/s observed, 2590 g/s predicted) and Bartow (1140 g/s observed, 1030 g/s predicted) are in excellent agreement with those derived from the continuous emission monitor (CEM) data. Inaccuracies in the relatively unsophisticated Gaussian plume model used, herein, are to be expected, especially, because it included neither terms for reflection

at the surface or at the boundary layer height. Note that predictions made with U.S. EPA's CALPUFF model also suggest that the influence of Bartow on ambient SO$_2$ concentrations at Sydney was relatively small for the same study period (13 May), whereas that for Gannon was much larger [*Poor et al.*, 2003].

[28] As indicated in Figure 5, the plume from Big Bend (station angle 220°; distance 25 km) arrived at Sydney at approximately 1230 LT and peaked at 1300 LT, before moving away from the site by 1400 LT. For this plant, $\chi/Q^{PDRM}s$ were larger (indicating less dilution) than $\chi/Q^{Met}s$ were during the period of plume influence, i.e., the opposite behavior as that observed for Gannon and Bartow. Presumably, this is an effect of Big Bend's much taller stack height (150 m) for which larger dilutions are predicted by the Met model. However, apparently, the plume was more coherent as evidenced by the excellent agreement between SO$_2$ emissions predicted by the PDRM and the CEM-derived value (i.e., 320 and 300, respectively; see Table 3). For the more distant Manatee plant (196°, 41 km), the χ/Q^{PDRM} and χ/Q^{Met} were nearly identical. The mean SO$_2$ emission rate predicted with the former (1140 g/s predicted, 1360 g/s observed) based on the average of the 18 ER$_{j,t}$ and the average CEM-derived rates, i.e., both averaged over the entire 9-hour study period) is about 20% lower than observed. However, inspection of Figures 3 and 5 suggests that during the time of plume influence (i.e., somewhat before 1200–1300 LT) the average observed SO$_2$ emission rate was indeed less than the study period average, which was affected by an increase later in the day, but after the plume had moved away from the site. Calculated on the basis of the period of plume influence, the observed SO$_2$ emission rate is 1110 g/s, i.e., within 3% of the PDRM prediction of 1140 g/s (see Table 3). Clearly, averaging times for these comparisons need to be considered in the model, but the model is, again, shown to be extraordinarily accurate.

[29] For the two smaller plants, Cargill and Gulf Coast (235° and 269°; 20 and 15 km, respectively), χ/Q^{PDRM} also exceeded χ/Q^{Met} values. This was especially true for Gulf Coast. As mentioned above, annual SO$_2$ emission rates for these sources were typically more than tenfold less than those for the four utility plants. As indicated in Table 3, the predicted average SO$_2$ emission rates (130 and 340 g/s, respectively) were threefold and twelvefold larger than their respective annual averages (40 and 25 g/s) obtained using emission factors (U.S. EPA 1998 emission inventory data), but the validity of these obtained emission rates cannot strictly be evaluated for these plants as only their annual SO$_2$ emission rates were available. Note that when χ/Q for these plants were constrained separately as described above, far better agreement between their predicted (49 and 31 g/s, respectively) and reported annual emission rates was achieved, and that for the 4 large power plants also improved somewhat (see Table 3).

[30] Despite its small SO$_2$ emission rate, Gulf Coast is a major Pb emission source. The plant recycles Pb-acid batteries into Pb ingots. Aluminum or other metals (i.e., Sb or As) are sometimes added to the ingots. During this study period, the occurrence of highly elevated fine-particle Al concentrations (>70 ng/m^3) together with Pb is, therefore, indicative of emissions from the Gulf Coast plant.
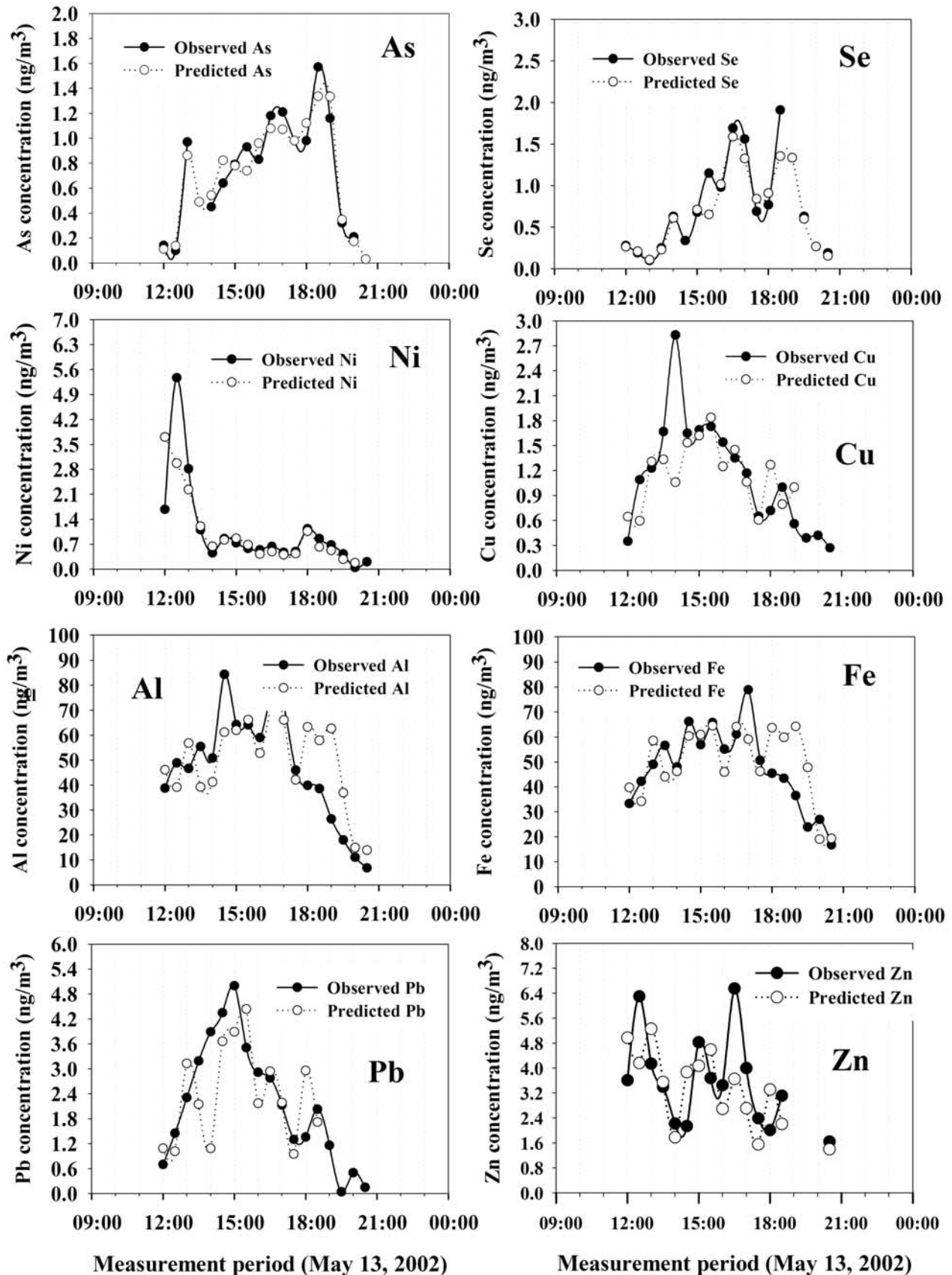
Figure 7. Observed and PDRM-predicted soncentrations of elemental species.

Table 4. Performance Statistics Between Observed and Predicted Concentrations for SO_2 and Metal Species[a]

	Units	SO_2[b]	Al	As	Cr	Cu	Fe	Mn	Ni	Pb	Se	Zn
Observed (average)	ng/m³	57.17	47.13	0.78	1.15	1.28	47.61	0.82	1.23	2.64	0.84	3.56
Predicted (average)	ng/m³	57.26	49.75	0.77	1.12	1.16	49.89	0.82	1.09	2.39	0.76	3.32
Ratio (average)	–	1.00	1.22	1.02	1.01	1.04	0.95	1.07	0.99	1.00	0.96	0.99
MB	ng/m³	−0.08	−2.62	0.01	0.03	0.12	−2.28	0.00	0.13	0.25	0.08	0.25
MNB	%	−6.5	−22.4	−2.1	−1.0	−4.4	−10.2	−3.3	1.1	−0.25	3.3	0.5
MFB	%	−2.7	−12.6	−0.6	2.0	3.5	−5.4	0.0	7.5	9.0	5.1	7.0
MAGE	ng/m³	4.74	11.7	0.10	0.24	0.33	10.1	0.16	0.47	0.82	0.14	1.1
MNGE	%	17.6	37.0	15.4	21.1	30.2	25.3	20.9	28.3	28.1	13.4	32.4
RMSE	ng/m³	6.24	14.77	0.12	0.29	0.53	12.74	0.19	0.88	1.06	0.23	1.32
NMSE	%	0.9	8.4	2.0	6.2	17.8	6.4	5.0	35.6	15.9	5.8	12.7
Fa2	%	94	83	100	100	93	94	100	93	93	100	100
CC	–	0.98	0.73	0.96	0.52	0.51	0.65	0.82	0.72	0.61	0.94	0.51

[a]MB, mean bias ($= (1/N) \sum_{i=1}^{N} (O_i - P_i)$); MNB, mean normalized bias ($= (1/N) \sum_{i=1}^{N} [(O_i - P_i)/O_i]$); MFB, mean fractional bias ($= (2/N) \sum_{i=1}^{N} [(O_i - P_i)/(O_i + P_i)]$); MAGE, mean absolute gross error ($= (1/N) \sum_{i=1}^{N} |O_i - P_i|$); MNGE, mean normalized gross error ($= (1/N) \sum_{i=1}^{N} [|O_i - P_i|/O_i]$); RMSE, root-mean-square error ($= [(1/N) \sum_{i=1}^{N} (O_i - P_i)^2]^{1/2}$); NMSE, normalized mean square error ($= [(1/N) \sum_{i=1}^{N} (O_i - P_i)^2]/[(1/N) \sum_{i=1}^{N} (O_i P_i)]$); Fa2, fractions of the predictions within a factor of 2 of the observed values; and CC, coefficient of correlation (R).

[b]SO_2 concentration variables are given in µg/m³.

Comparison of Figures 5 and 7 shows that Al excursions are better correlated with periods when the plume from Gulf Coast influenced Sydney than any of the power plants, including Gannon and Bartow, for which Al-containing fly ash emissions might be expected. Moreover, the ambient concentration profiles for Pb and Al are reasonably well fit by the six-source model. Taken together, all of this information suggests that χ/Q^{PDRM} predictions using the modified constraints are, in fact, reasonably accurate. A more detailed evaluation of PDRM performance is given below.

4.2. Elemental Constituents

[31] The order of appearance of the plumes from the six sources is easily seen from their ambient concentration time series plots shown in Figure 7. The concentration of Ni, an important tracer of fuel oil combustion, is first seen peaking ($\sim$5.5 ng/m³) between 1200 and 1300 LT, in agreement with the maximum χ/Q^{PDMR} for Manatee, a large OFPP, and the second largest SO_2 emitter of the six sources used in the model. Very minor Ni excursions are indicated at 1430, 1630, and 1800 LT in accordance with χ/Q^{PDMR} maxima for Bartow (Figure 5), which also operated oil-fired units, at precisely those times.

[32] The dispersion plot (Figure 5) shows that Big Bend's, a large but well-controlled (ESP and wet lime scrubber) influence was confined to a brief period centered about 1300 LT. As shown in Figure 6 and discussed above, it had only a small effect on SO_2 concentrations observed at Sydney and a negligible effect on that of Se, a nearly unique tracer of primary particles from coal combustion. Its small influence on Se concentrations is consistent with its control technology, as wet scrubbers are known to also scrub gas-phase Se [Ondov et al., 1979], in which substantial fractions of the Se emission often resides [Ondov et al., 1989]. Arsenic, coemitted with Se during coal combustion, however, did peak at 1300 LT, in accordance with the arrival of the Big Bend plume at Sydney. As shown in Figure 7, Se peaked at 1400, 1530, and 1830 LT, in accordance with plumes from coal-fired boilers at Gannon and Bartow. Arsenic concentrations were likewise

elevated at 1530, 1630, and 1830–1900 LT, in good agreement with the arrival of plumes from the Gannon and Bartow plants. The ratio of As to Se in airsheds influenced by coal combustion is $\sim$1. Between 1200 and 2030 LT this ratio ranged from 0.70 to 2.00 with a mean of 1.23 ± 0.43, i.e., in agreement with a coal combustion source.

[33] Peaks in ambient Al, Fe, Zn, and Cu were also evident at 1630 LT as well as 1830 LT, but at reduced size. In general, concentration time series are more difficult to interpret for these elements, as there are many sources and analytical and sampling errors tended to be larger, especially, for Al and Fe, when their concentrations are dominated by dust particles, which can be trapped in the solenoid value in the SEAS or be excluded from the small aliquots of sample actually analyzed. The latter process may account for overprediction of Al and Fe between 1800 and 1930 LT. Peaks in the time series plots for Zn, and to a lesser extent, Cu and Al, occur at 1230 LT, along with Ni, suggesting influence from Manatee.

[34] Copper is clearly underpredicted at 1230 LT and more so at 1400 LT, possibly as a result of an additional source. Likewise, Al was underpredicted at 1430 LT, and Zn was substantially underpredicted at 1630 LT, i.e., when Gannon and Bartow plumes were influencing the site. The underprediction of Zn may be due to the influence of a small incinerator, about 10 km from the site at a station angle of 250°. The plume from this incinerator was clearly observed on 17 May.

[35] Lead peaks were observed at 1300 LT, in accordance with the arrival of the Big Bend plume and, later, between 1450 and 1530 LT, when maximum influence from the Gulf coast plume was predicted by the PDRM. Lead concentrations also peaked at 1630 LT, and again at 1800–1900 LT, in accordance with arrival of the Gulf Coast plume.

4.3. Performance Measures

[36] Receptor model performance is often discussed in terms of ratios of predicted and observed values. However, several additional measures have been used to evaluate air quality models [Londergan et al., 1983; Londergan and
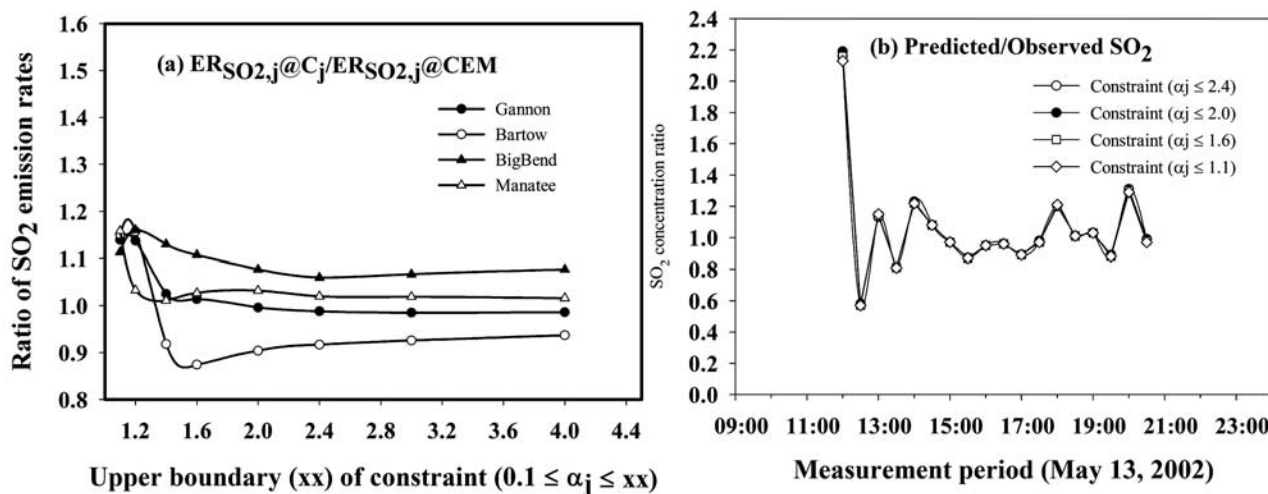
Figure 8. Results of sensitivity analysis case 1: all sources constrained identically. (a) Ratios of predicted and observed SO_2 emission rates for different upper bound constraints. (b) Ratios of predicted and observed SO_2 concentrations for different constraints on the upper bound.

Wackter, 1984; *Hanna*, 1988; *Kumar et al.*, 1993; *Patel and Kumar*, 1998; *Kumar et al.*, 1999] and are defined in Table 3. These include measures of differences between predicted and observed values (e.g., normalized mean square error (NMSE) and mean fractional bias (MFB)), correlation coefficients, and the fraction of predictions within a factor of 2 of observations (Fa2). According to *Kumar et al.* [1993], model performance is deemed acceptable if NMSE ≤ 0.5, −0.5 ≤ MFB ≤ 0.5, and Fa2 ≥ 0.8 (80%).

[37] Herein, the ratios of the predicted and observed average concentration were 1.00 ± 0.18 in SO_2, 1.02 ± 0.18 ($0.8\sim1.4$) for As, 0.96 ± 0.17 ($0.6\sim1.2$) for Se, and 0.99 ± 0.41 ($0.6\sim2.2$) for Ni, respectively. Highest (2.2) and lowest (0.6) ratios in the Ni component observed between 1200 and 1300 LT time zones might be due to uncertainty for the fluctuation in the wind angles. Residuals ranged from -15.6 to 10.4 $\mu g/m^3$ (mean bias: -0.08 $\mu g/m^3$, see Table 4) for SO_2, -0.18 to 0.14 ng/m^3 (mean bias: 0.01 ng/m^3) for As, from -0.15 to 0.56 ng/m^3 (mean bias: 0.08 ng/m^3) for Se, and from -2.0 to 2.5 ng/m^3 (mean bias: 0.13 ng/m^3) for Ni. As indicated in Table 4, MNB range from -2.1% for As to 3.3% for Se. The performance indices, NMSE, MFB, and Fa2, are also quite reasonable for these three markers, ranging from 2.0, -0.6, and 100% for As to 35.6, 7.5, and 93% for Ni. The mean normalized gross error (MNGE, also defined in Table 4) ranged from 13.4% for Se to 28.3% for Ni. For the metals species showing temporal concentration profiles similar to that of SO_2, i.e., As, Se, and Ni, the agreement between predicted and observed concentrations was excellent, as shown in Figure 7 and Table 4.

[38] Poorer agreement was observed for the other elements, which as discussed above, we attribute to other sources and, in the case of Fe and Al, sampling losses. Another factor to consider is that source profiles and hence emission rates for particle constituents may not be constant in time, especially, over such short time periods,

and might change differently than those for SO_2, as particles and SO_2 are subject to different control technology. Additionally, the model results are largely driven by the temporal SO_2 concentration profiles, because SO_2, present at tens of $\mu g/m^3$ levels, was the single most abundant species. Thus even small relative differences between calculated and observed values for SO_2 represent a large fraction of the least squares sum of the differences (equation (3)) which is to be minimized in the model.

[39] For Al, the average ratio of predicted to observed levels was 1.22 ± 0.50 ($0.7\sim2.4$); and 0.95 ± 0.15 ($0.7\sim2.0$) for Fe; 1.07 ± 0.33 ($0.7\sim1.8$) for Mn; 1.04 ± 0.43 ($0.4\sim1.9$) for Cu; 1.00 ± 0.47 ($0.3\sim2.2$) for Pb; and 0.99 ± 0.39 ($0.6\sim1.8$) for Zn. Overpredictions for crustal elements, Al and Fe, were $50\sim200\%$ between 1800 and 2000 LT for reasons discussed above. As indicated in Table 4, MNB
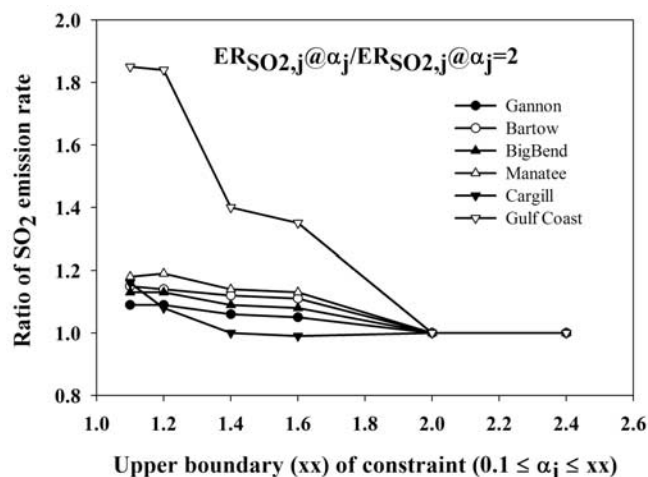

Figure 9. Normalized emission rate predicted as a function of the value of the base upper bound constraint, wherein separate constraints are applied for the Cargill and Gulf Coast plants.

ranged from −22.4 to 3.3% depending on the metals species. Both errors and performance indices (NMSE, MFB, and Fa2) associated with the model predictions are also varied, depending upon species, but the indices are all within the acceptable ranges.

[40] Emission rates predicted for the 10 particle constituents and for each of the six sources are also listed in Table 3. However, to validate these results, in-stack monitoring should be done for at least one of the emission sources.

[41] As indicated in Figure 7, the SO_2 concentration profile predicted by the six-source model is in excellent agreement with the observed SO_2 concentrations. Regression of observed and predicted concentrations (excluding observations for which measurement uncertainty exceeded 30%) gave a slope of 0.965, an intercept of 0.002 ($\mu g/m^3$), and correlation coefficient (R^2) of 0.969. As indicated in Table 4, the average observed SO_2 concentration (57.2 $\mu g/m^3$) is nearly identical to the predicted average (57.3 $\mu g/m^3$), and the mean normalized bias (MNB), which is sensitive to small observed concentrations, is −6.5%. Additionally, NMSE, MFB, and Fa2 for SO_2 are 0.9, −2.7, and 94%, respectively, which are within the acceptable ranges suggested by *Kumar et al.* [1993]. Last, the mean normalized gross error (MNGE), which like the MNB is sensitive to small observed concentrations, is low (17.6%). These performance measures suggest that the PDRM, coupled with highly time-resolved ambient measurements, could be effectively used as a tool to remotely monitor emission rates of SO_2, develop dispersion models, and estimate emission rates of toxic and other noncriteria pollutants without expensive in-stack monitoring.

4.4. Sensitivity to Constraints

[42] Two sets of sensitivity analyses were performed. The first was conducted for the base case in which all six sources were identically constrained and UB was varied from 1.0 to 8.0. Results are shown in Figure 8a, wherein the ratio of predicted to observed average SO_2 emission rates are plotted against UB. In this case, results for Cargill and Gulf Coast are not shown because CEM data are not available. As shown in Figure 8a, there is little change in the ratio of the observed and predicted SO_2 emission rates for UBs exceeding 2.0. Ratios for UB < 2.0 increased somewhat but remained in the range 0.88 to1.16 depending on the source. Clearly, larger UBs are favored. As shown in Figure 8b, the predicted ambient SO_2 concentrations are insensitive to the choice of the UB constraint. As discussed above, there are good reasons to expand constraints applied to the χ/Q for Cargill and Gulf Coast. In Figure 9, the effect of UB on model results are shown for the case wherein UBs for Cargill and Gulf Coast are set to 4 and 12 times those for the base constraint set for the other plants. In this figure, the predicted emission rates are normalized to those calculated for the base constraint = 2 (i.e., for which upper bounds for χ/Q^{PDRM} are 2 × 4 = 8 and 2 × 12 = 24 for Cargill and Gulf Coast, respectively). For values of the base constraint >2, there is no change in the predicted values for any of the plants. As the upper bound of the base constraint is decreased from 2 to 1.1, predicted emissions change by <20% for all plants except Gulf Coast. Clearly, the choice of constraint is most sensitive for Gulf Coast, but given that there is little change in model predictions for upper bounds

>2 × 12, and that the emission rate predicted at this upper bound is in better agreement with the annual emission rate, this would seem a logical choice. As noted above, constraining UBs for Cargill and Gulf Coast leads to better agreement between predicted and observed values for the larger plants (see Table 3).

5. Concluding Remarks

[43] A hybrid model, combining features of least squares mass balance receptor and deterministic Gaussian plume models, has been applied to highly time-resolved ambient SO_2 and primary aerosol components measured during the BRACE to predict their contributions to ambient levels from known stationary sources. Unlike factor analysis and traditional chemical mass balance models, the new model was designed to directly make use of the numbers and locations of known sources, their geographic relation to the receptor site, and wind direction during sampling. Results encompass average emission rates of primary pollutants from specific, individual sources, meteorological dispersion factors (χ/Q) for each source, and the ambient concentrations induced at the receptor site by the modeled sources. Emission rates determined for individual sources can be readily tested against in-stack measurements. Furthermore, accurate solutions were obtained for six sources with data for only 18 observational periods. In contrast, factor analysis models require much larger data sets, i.e., wherein, by one estimate, the number of observations must exceed the number of variables (elements) by 50 if stable results are to be obtained [*Thurston and Spengler*, 1985].

[44] Model predictions were extraordinarily accurate for SO_2 emissions from the four sources for which accurate emission data were available during the modeling period. This was true even though two of the plants, Gannon and Big Bend, lay along almost identical station angles and are separated by a distance of only 18 km. Furthermore, predicted concentrations for elemental constituents of emitted particles well accounted for concentrations of elemental constituents, especially, well-known marker species (As, Se, and Ni). On the basis of these and other quantitative performance measures presented above, we conclude that the PDRM, coupled with highly time-resolved ambient measurements, could be effectively used as a tool to remotely monitor emission rates of SO_2, develop dispersion models, and estimate emission rates of toxic and other noncriteria pollutants without expensive in-stack monitoring.

[45] Clearly, the PDRM will need to be tested in more complex emission source environments and against more complete emission data before we can fully appreciate its value and limitations.

References

Binkowski, F. S. (1979), A simple semi-empirical theory for turbulence in the atmospheric surface layer, *Atmos. Environ.*, 13, 247–253.

Briggs, G. A. (1969), Plume rise, *Crit. Rev. Ser. T/D 25075*, U.S. At. Energy Comm., Washington, D. C. (Available from Natl. Tech. Inf. Serv., Springfield, Va.)

Briggs, G. A. (1971), Some recent analyses of plume rise observations, in *Proceedings of the Second International Clean Air Congress*, edited by H. M. Englund and W. T. Beery, pp. 1029–1032, Elsevier, New York.

Briggs, G. A. (1974), Diffusion estimation for small emissions, in *Environmental Research Laboratories Air Resources Atmospheric Turbulence and Diffusion Laboratory 1973 Annual Report*, USAEC Rep. ATDL-106, NOAA, Washington, D. C.

Cooper, D. W. (1982), Receptor-oriented source-receptor analysis, paper presented at Specialty Conference on Receptor Models Applied to Contemporary Pollution Problems, Northeast Atl. Int. Sect. of the Air Pollut. Control Assoc., Danvers, Mass., 17–20 Oct.

Draxler, R. R. (1976), Determination of atmospheric diffusion parameters, *Atmos. Environ.*, 10, 99–105.

Gifford, F. A. (1961), Use of routine meteorological observations for estimating, atmospheric dispersion, *Nucl. Safety*, 2, 47–51.

Gordon, G. E. (1988), Receptor models, *Environ. Sci. Technol.*, 22, 1132–1142.

Hanna, S. R. (1988), Air quality model evaluation and uncertainty, *JAPCA*, 38, 406–412.

Hanna, S. R., R. Britter, and P. Franzese (2003), A baseline urban dispersion model evaluated with Salt Lake City and Los Angeles tracer data, *Atmos. Environ.*, 37, 5069–5082.

Henry, R. C. (1987), Current factor analysis models are ill-posed, *Atmos. Environ.*, 21, 1815–1820.

Henry, R. C. (2000), UNMIX theory and applications, in *Final Report of Workshop on UNMIX and PMF as Applied to PM$_{2.5}$*, Publ. EPA/600/A-00/48, edited by R. D. Willis, pp. 4–6, U.S. Environ. Prot. Agency, Washington, D. C.

Henry, R. C., and G. A. Norris (2002), *EPA UNMIX 2.3 User Guide*, Natl. Exposure Res. Lab., U.S. Environ. Prot. Agency, Research Triangle Park, N. C.

Henry, R. C., E. S. Park, and C. H. Spiegelman (1999), Comparing a new algorithm with the classical methods for estimating the number of factors, *Chemom. Intel. Lab. Syst.*, 48, 91–97.

Irwin, J. S. (1979), Scheme for estimating dispersion parameters as a function of release height, *Publ. EPA-600/4-79-062*, U.S. Environ. Prot. Agency, Washington, D. C.

Kidwell, C. B., and J. M. Ondov (2001), Development and evaluation of a prototype system for collecting sub-hourly ambient aerosol for chemical analysis, *Aerosol Sci. Technol.*, 35, 596–601.

Kidwell, C. B., and J. M. Ondov (2004), Elemental analysis of sub-hourly ambient aerosol collections, *Aerosol Sci. Technol.*, 38, 205–218.

Kim, B. M., and R. C. Henry (2000), Application of the SAFER model to Los Angeles PM$_{10}$ data, *Atmos. Environ.*, 34, 1747–1759.

Kumar, A., J. Luo, and G. Bennett (1993), Statistical evaluation of lower flammability distance (LFD) using four hazardous release models, *Process Safety Prog.*, 12, 1–11.

Kumar, A., N. K. Bellam, and A. Sud (1999), Performance of an industrial source complex model: Predicting long-term concentrations in an urban area, *Environ. Prog.*, 18, 93–100.

Lioy, P. J., M. P. Zelenka, M. D. Cheng, N. M. Reiss, and W. E. Wilson (1989), The effect of sampling duration of the ability to resolve source types using factor analysis, *Atmos. Environ.*, 23, 239–254.

Londergan, R. J., and D. J. Wackter (1984), Evaluation of complex terrain air quality simulation models, *Publ. EPA-450-4-84-017*, U.S. Environ. Prot. Agency, Research Triangle Park, N. C.

Londergan, R. J., D. H. Minott, D. J. Wackter, and R. R. Fizz (1983), Evaluation of urban air quality simulation models, *Publ. EPA-450-4-83-020*, U.S. Environ. Prot. Agency, Research Triangle Park, N. C.

Ondov, J. M., R. C. Ragaini, and A. H. Biermann (1979), Elemental emissions from a coal-fired power plant: Comparison of a Venturi wet scrubber system with a cold-side electrostatic precipitator, *Environ. Sci. Technol.*, 13, 598–607.

Ondov, J. M., C. E. Choquette, W. H. Zoller, G. E. Gordon, A. H. Biermann, and R. E. Heft (1989), Atmospheric behavior of trace elements on particles emitted from a coal-fired power plant, *Atmos. Environ.*, 23, 2193–2204.

Ondov, J. M., W. R. Kelly, J. Z. Holland, Z. Lin, and S. A. Wight (1992), Tracing fly ash emitted from a coal-fired power plant with enriched rare-earth isotopes, *Atmos. Environ., Part B*, 26, 453–462.

Ondov, J. M., J. P. Pancras, S. Gazula, M. Yu, J. Turner, A. Robinson, S. Pandis, N. D. Poor, and R. K. Stevens (2003), Highly time-resolved measurements of elemental composition at the Baltimore, St. Louis, Pittsburgh, and Tampa Supersites using the UM high-frequency aerosol slurry sampler: Unprecedented resolution of the sources of primary atmospheric aerosol, paper presented at 2003 PM AAAR Meeting, Am. Assoc. for Aerosol Res., Pittsburgh, Pa., 31 March to 4 April.

Paatero, P. (1997), Least square formulation of robust non-negative factor analysis, *Chemom. Intel. Lab. Syst.*, 37, 23–35.

Paatero, P. (1999), The multilinear engine: A table-driven, least squares program for solving multilinear problems, including the *n*-way parallel factor analysis model, *J. Comput. Graph. Stat.*, 8, 854–888.

Pancras, J. P. (2005), Multielement electrothermal AAS determination of eleven marker elements in fine ambient aerosol slurry samples collected with SEAS-II, *Anal. Chim. Acta.*, in press.

Panofsky, H. A., A. K. Blackadar, and G. E. McVehil (1960), The diabatic wind profile, *Q. J. R. Meteorol. Soc.*, 86, 390–398.

Pasquill, F. (1961), The estimation of the dispersion of windborne material, *Meteorol. Mag.*, 90, 33–49.

Patel, V. C., and A. Kumar (1998), Evaluation of three air dispersion models: ISCT2, ISCLT2, and SCREEN2 for mercury emissions in an urban area, *Environ. Monit. Assess.*, 53, 259–277.

Poor, N., C. Amalfilano, J. Ondov, P. Pancras, S. Gazula, P. Dasgupta, and R. Al-Horr (2003), Real-time monitoring of gases and aerosols reveals source contributions, paper presented at NARSTO Workshop on Innovative Methods for Emission-Inventory Development and Evaluation, NARSTO, Austin, Tex., 14–17 Oct.

Rheingrover, S. W., and G. E. Gordon (1988), Wind-trajectory method for determining compositions of particles from major air pollution sources, *Aerosol Sci. Technol.*, 8, 29–61.

Schwede, D. B., and J. O. Paumier (1987), Sensitivity of the industrial source complex model to input deposition parameters, *J. Appl. Meteorol.*, 36, 1096–1106.

Scire, J. S., R. R. Francoise, M. E. Fernau, and R. J. Yamartino (2000), *A User's Guide for the CALMET Meteorological Model (Version 5)*, Earth Tech, Inc., Concord, Mass.

Thurston, G. D., and J. D. Spengler (1985), A quantitative assessment of source contributions to inhalable particulate matter pollution in metropolitan Boston, *Atmos. Environ.*, 19, 9–25.

U.S. Environmental Protection Agency (U.S. EPA) (1980), Guidelines on air quality models, *OAQPS Guideline Ser.*, Research Triangle Park, N. C.

U.S. Environmental Protection Agency (U.S. EPA) (1995), *User's Guide for the Industrial Source Complex (ISC3) Dispersion Models*, vol. II, *Description of Model Algorithms*, Research Triangle Park, N. C.

Wahlin, P. (2003), COPREM: A multivariate receptor model with a physical approach, *Atmos. Environ.*, 37, 4861–4867.

Yamartino, R. J. (1982), Formulation and application of a hybrid receptor model, paper presented at Specialty Conference on Receptor Models Applied to Contemporary Pollution Problems, Northeast Atl. Int. Sect. of the Air Pollut. Control Assoc., Danvers, Mass., 17–20 Oct.

————————————

J. Ondov and J. P. Pancras, Department of Chemistry and Biochemistry, University of Maryland, College Park, Chemistry Building 91, College Park, MD 20742, USA. (jondov@umd.edu)

S. S. Park, Department of Environmental Engineering, Chonnam National University, 300 Yongbong-dong, Buk-ku, Gwangju 500-757, Korea.

N. Poor, Department of Environmental and Occupational Health, College of Public Health, University of South Florida, Tampa, FL 33612, USA.
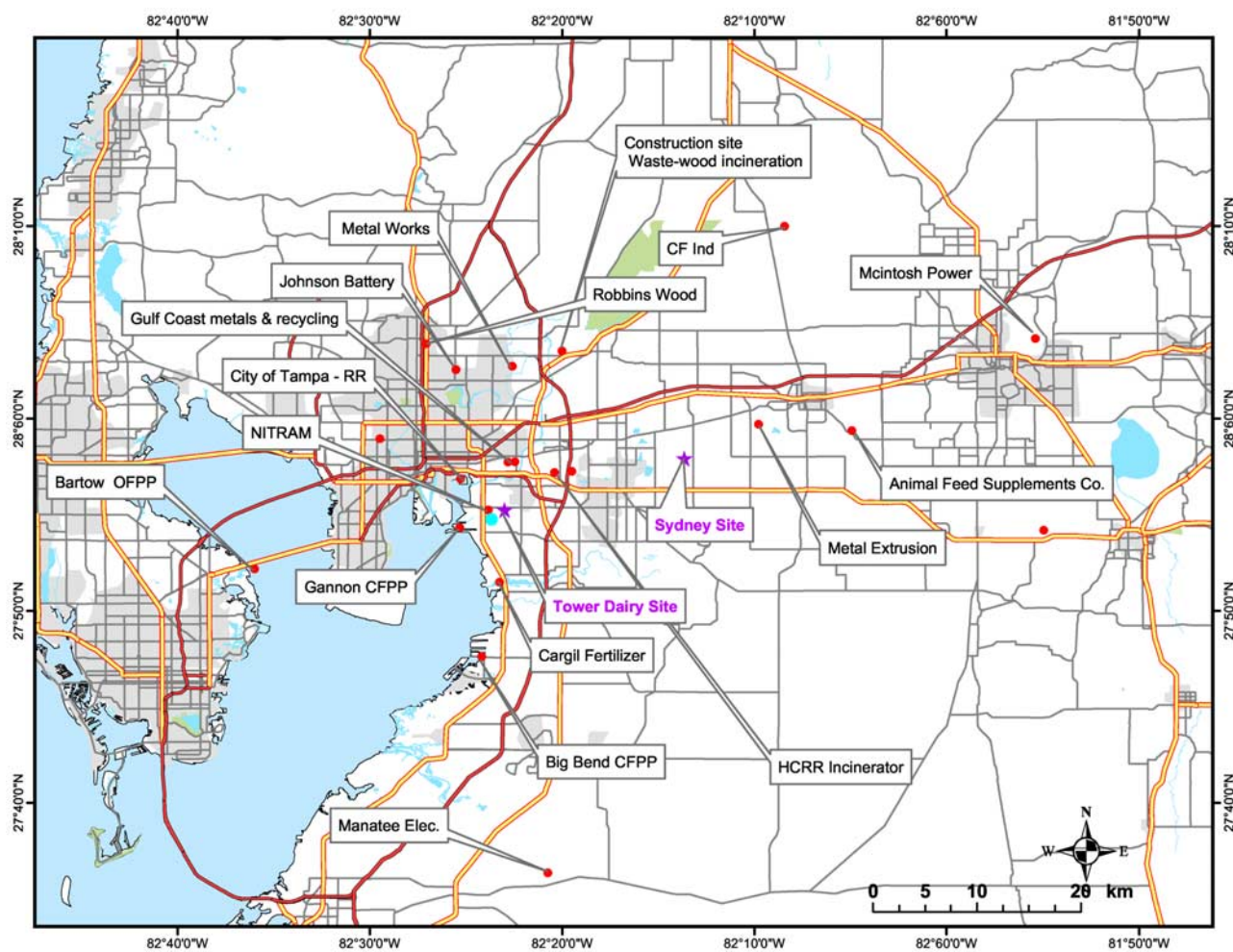
Figure 1. Area map showing the Sydney sampling site and nearby air emission sources.